Study of the irradiation hardening of a Fe9Cr ferritic model alloy by nanoindentations

D. Zhou, P. Spätig, Q. Hayat, P. Song, N. Jennett, J.-C. Chen, P. Desgardin

Nuclear Materials and Energy 39 (2024) 101667

Contents lists available at ScienceDirect

Nuclear Materials and Energy

journal homepage: www.elsevier.com/locate/nme

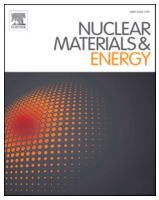

Study of the irradiation hardening of a Fe9Cr ferritic model alloy by nanoindentations

D. Zhou [a,b], P. Spätig [a,c,*], Q. Hayat [d], P. Song [a], N. Jennett [e], J.-C. Chen [a], P. Desgardin [f]

[a] Paul Scherrer Institut (PSI), Nuclear Energy and Safety Research Department (NES), Laboratory for Nuclear Materials (LNM), CH-5232 Villigen PSI, Switzerland
[b] Nuclear Power Institute of China, Chengdu 610213, China
[c] Laboratoy for Reactor Physics and Systems Behaviour, École polytechnique fédérale de Lausanne(EPFL), CH-1015 Lausanne, Switzerland
[d] Warwick Manufacturing Group, University of Warwick, Coventry, United Kingdom
[e] Strategic Measures Consultancy Ltd, United Kingdom
[f] CEMHTI, CNRS, UPR3079, University of Orléans, F-45071 Orléans, France

ARTICLE INFO

Keywords:
Fe-Cr model alloy
Nano-indentations
Indentation size effect
Structural size effects
Proton irradiation
Irradiation hardening

ABSTRACT

This paper presents a series of Berkovich indentation results obtained on unirradiated and 7.2 MeV proton irradiated specimens of a Fe9Cr model alloy with an equiaxed ferritic microstructure. Using a energy degrader wheel made of 24 aluminum foils of different thickness, a flat damage profile of about 50 μm resulted from the irradiation, allowing to perform indentations within a volume material that is homogeneously irradiated. The indentation size effect on measured hardness was analyzed with a model based on the disloction-slip distance theory built on the concept of combined spatial frequency of all obstacles to dislocation motion. The effects on hardness of the tip-specimen contact size (or penetration depth), dislocation density and mean distance between irradiation defects were quantified and discussed. The irradiation hardening was characterized by the increase of hardness determined at large penetration depths.

1. Introduction

"Ferritic" steels (=ferritic, bainitic, martensitic steels) are used for structural components in the currently operating nuclear power plants [1]. As the next generation of nuclear power plants will operate at high temperatures, the performance of these steels has to be improved, which is largely realized through fundamental investigations, where the chemical composition and thermo-mechanical treatment are being optimized, and advanced oxide-dispersion strengthened steels developed. For the current ageing fission reactors, as well as for those of the next generation, a crucial point is to assess the degradation of the mechanical properties induced by neutron irradiation and to improve their radiation resistance. As a consequence, investigations on neutron-irradiated materials are required to measure the irradiation hardening (increase of flow stress) and embrittlement (decrease of toughness) [2]. However, neutron irradiation facilities are few and irradiations are very costly. In addition, handling and testing radioactive standard specimens, which are relatively big, can be done only in a limited number of hot laboratories equipped with the appropriate hot cells and shielded testing devices. Thus, over the years, ion beam irradiations have been considered as surrogate to neutron ones [3,4] or to charge specimens with helium [5]. However, the penetration depth of heavy ions up to 100 MeV remains lower than 10 μm in steel; protons with that energy penetrate deeper in steel, up to 1 cm. In addition, for mono-energetic ion beams, the resulting damage profile presents a strong gradient. Hence, to determine the change in material strength following ion irradiations, micro-mechanical testing sampling a tiny amount of materials is inevitable. Nano- and micro-indentation experiments have long been used for this purpose.

This study was launched to address the possibility of extracting reliable mechanical material properties from indentation tests, where the underlying physics of size effect and length scale associated with indentation is far from being well understood and unified. The proposed work consisted of performing a series of indentations using a geometrically self-similar indenter tip (Berkovich) on a pure Fe9Cr equiaxed grain ferritic alloy in unirradiated and irradiated conditions with 7.2 MeV protons. Indentation tests were carried out over a range of depth (0.5 to 6 μm) to separate the intrinsic indentation size effect from the structure size effect on the measured hardness. Furthermore, considering the characteristics of the Fe9Cr alloy along with the indented

* Corresponding author at: Department of Nuclear Energy and Safety, Paul Scherrer Institute, 5232 Villigen, Switzerland.
E-mail address: philippe.spatig@psi.ch (P. Spätig).

https://doi.org/10.1016/j.nme.2024.101667
Received 10 November 2023; Accepted 28 April 2024
Available online 30 April 2024

plastic size permitted to separate the respective contribution of these features to the hardness, and so was done for the irradiation defects by comparison of the tests on specimens in the unirradiated and irradiated conditions.

2. Background on the modified dislocation slip-distance theory

Nowadays, it well established that, when using geometrically self-similar indenters (pyramids or cones), the hardness decreases with the penetration depth referred. Nix and Gao [6] proposed a model based on dislocations where so-called geometrically necessary dislocations (GND) must be present to accommodate the strain gradient below the indenter tip. GND provide an extra contribution to the flow stress through Taylor's equation [7], which would be otherwise related only to statistically stored dislocations in the absence of strain gradient. This model predicts an indentation size effect (ISE) for geometrically self-similar indenters that is given by:

$$\frac{H}{H_o} = \sqrt{1 + \frac{h^*}{h}} \tag{1}$$

where H_o represents the hardness at an infinite depth, h the penetration depth and h* is a characteristic length depending on the material and indenter geometry.

For nano-indentation (to be understood as indentation depth smaller than 100 nm), Nix and Gao models breaks down, because below this depth, the self-similarity of a real indenter is lost due to tip blunting. Huang et al. [8] developed a similar model to Nix and Gao model but they introduce a maximum allowable GND density, which arises from the strong repulsive force between dislocations. A similar approach was considered for non-geometrically self-similar indenter, like spherical indenter, where again the size effect is related to the indenter radius rather than the contact depth. While the Nix-Gao model has become the standard model to explain ISE, it is not free of inconsistency with microstructural observations. In particular, it is not fully compatible with measurement of GND under indent imprints. Indeed, the work of Demir et al. [9] on copper single crystals revealed that GND do not form homogeneous arrangements but are observed as patterns. More important is the fact that the density of GND was not found to increase with decreasing indentation depth as modeled in Nix-Gao approach, but on the contrary it decreases. This observation is in frontal contradiction with the strain-gradient plasticity approach usually considered to explain ISE and that the sole distinction between statistically stored and geometrically necessary dislocations cannot account completely for the observed ISE. Thus, size effects in plasticity are not systematically related to strain-gradient. Following the work of Dunstan et al. [10], further developed by Hou and Jennett [11], ISE can also be associated with a general mean free path of moving dislocations D that represent the contribution of all obstacles to dislocations including grain size, forest dislocations, inclusions, carbides, as well as the size of plastic zone itself, leading to the idea that material strength is mediated simultaneously by structural size effects (SSE) and the size of the indent. From a series of measurement with spherical indenters on polycrystalline copper of various grain sizes, Hou et al. [11,12] showed that hardness, defined as the mean pressure $P_m = F/\pi a^2$ (F = applied force and a = contact radius), can be written as:

$$P_m = P_y + \sqrt{\frac{k_1}{a} + \frac{k_2}{d} + \sum_i \frac{k_i}{d_i}} = P_y + \frac{\widetilde{K}}{\sqrt{D}} \tag{2}$$

where P_y is the minimum stress to move a dislocation through the lattice, the Peierls stress which is not associated to any length scale, a is the indenter-material contact radius, d is the grain size, and d_i represents any other length that controls the dislocation mean free path, which can be associated with the spatial frequency of carbides or irradiation-induced defects for example. The constants k_i are scaling parameters.

3. Material

The investigated material of this study was a model alloy Fe-9 %Cr (wt. %) alloy, with the following chemical composition: 9.1Cr, 0.009Ni, 0.004Si, 0.003P, 0.027Al, and Fe for the balance. The alloy was thermally treated at ~ 950 °C for ~ 1800 s in air, subsequently cooled down to 790 °C at the very slow rate of ~ 0.04 °C/s, and then kept at 790 °C for ~ 86400 s (around 24 h). The final step was air-cooling. All steps are shown in Fig. 1. Relatively large equiaxed ferrite grains of 80 μm were formed. Prior to microstructural characterization and experimental indentation testing, all specimens were ground with SiC papers down to 4000 grits, followed by polishing with successive diamond pastes of 9, 6, 3 and 0.25 μm size at 100 rpm for 2–5 min at each step until the scratch from previous steps were completely removed. Then a chemical–mechanical polishing was applied to remove all scratches and deformation using an OP-S colloidal silica suspension with a pH of 9.8 and a grain size of about 0.04 μm at 50 rpm for 10 min. Finally, an electro-polishing with 5 % oxalic acid for 1–2 min was applied.

The grain morphologies of Fe9Cr were characterized by using electron back scatter diffraction (EBSD) technique within a ZEISS NVison40, which is equipped with a Schottky field emission gun. Fig. 2 shows an inverse pole figure, where different colors represent different crystal orientations, where one can see an equiaxed ferritic structure.

2.1. Proton irradiations at CEMHT/CNRS Orléans/France

7.2 MeV proton-irradiations were performed at CEMHTI/CNRS in Orléans/France. The main advantage of such irradiations resides in the relatively large penetration depth of the protons into the specimens. As shown in Fig. 3, a 50 μm thick layer can be irradiated.

The homogeneity of the irradiation is realized with the use of a 24 aluminum foils degrader wheel. With 7.2 MeV passing through a magnet scanning system and a degrader wheel with 24 Al-foils of variable thicknesses, the samples were 3D-homogeneously implanted. The production of displacement damage was calculated by SRIM code for displacement threshold energy of 40 eV and the damage cross section was calculated as $3.0\text{x}10^{-5}$ vac/(Å ion) (vacancy per Angstrom (Å) and impinging ion) with an average beam current density of 14 μA/cm^2, a displacement rate of about $3.18\text{x}10^{-6}$ dpa/s (displacements per atom per second). Two specimens were irradiated up to 0.2 and 0.5 dpa and the irradiation temperature remained lower than 150 °C.

2.2. Experimental tests of spherical indentation

The nano-indentation tests were performed with a nano-indenter (Agilent G200) using a Berkovich tip. Progressive multiple-cycle (PMC) in forced control was selected to determine the hardness as a function of the indentation depth. Five consecutive loading partial unloading segments were carried in a particular PMC cycle before reaching a maximum force F_{max} of either 60, 75 or 100 mN position. The load reached at the i^{th} cycle (i = 1 to 5) is given by:

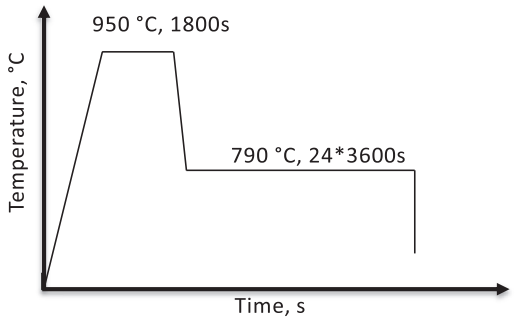

Fig. 1. Heat treatment to produce an equiaxed ferritic structure in Fe9Cr alloy.

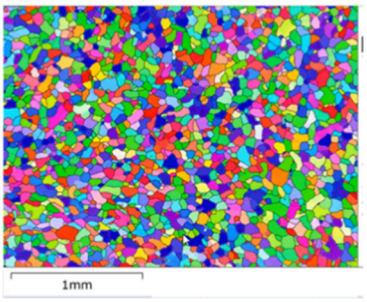

Fig. 2. EBSD inverse pole figure of Fe9Cr alloy.

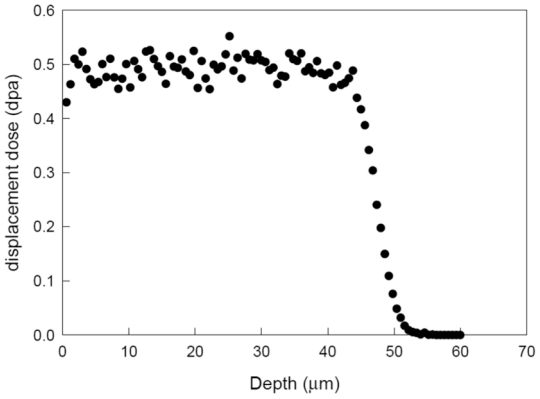

Fig. 3. Damage profile in the Fe9Cr alloy after the 7.2 MeV proton irradiations.

$$F_i = \frac{F_{\max}}{2^{(5-i)}} \tag{3}$$

For each condition at least one PMC with each of the three F_{max} was carried out, covering forces from 3.75 mN to 100 mN. An example of PMC up to 100 mN is shown in Fig. 4.

The unloading was set to 2 s where half of the load was removed after a dwell time of 38 s. This loading-dwell-unloading scheme was optimized to minimize creep effect to be as closed as possible to a fully elastic unloading. This is particularly important at F_i where the contact stiffness is used to calculate the hardness values. The tip area function was calibrated against the Young's modulus of a reference fused silica specimen using the Oliver and Pharr model [13]. We just recall here that Oliver and Pharr model, when applied to fused silica, assumed a sink-in behavior at the tip-specimen contact. However, for metallic material, the material behavior is better described by a pile-up. In other words, for a given penetration depth, the contact area is larger for metallic materials than for fused silica, which has to be accounted for. The reduced

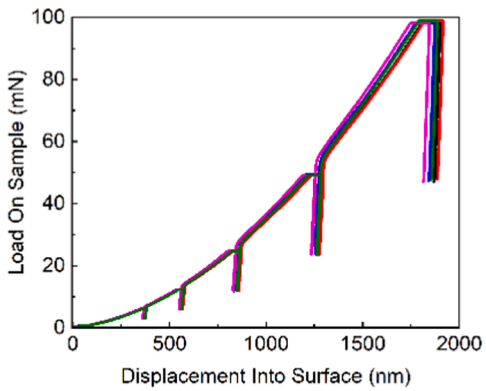

Fig. 4. Progressive multiple-cycle up to 100 mN.

Young's modulus E_r depends on the contact area A_c, and scales with the contact stiffness S as:

$$E_r^{measuresd} = \frac{\sqrt{\pi}}{2\beta}\frac{S}{\sqrt{A_c}} \qquad with \qquad \frac{1}{E_r} = \frac{(1-\upsilon_i^2)}{E_i} + \frac{(1-\upsilon_s^2)}{E_s} \tag{4}$$

where β is a geometric factor for the Berkovich indenter equal to 1.034, E_i and E_s are the Young's modulus and ν_i and ν_s are the Young's modulus and Poisson's ratio of the indenter and specimen, respectively. E_r measured usually differs significantly from the theoretical value, due to the uncertainty in A_c but also, and even more important, due to the high uncertainty in the stiffness S that stems from small error in the frame compliance and small thermal or creep drift. The method adopted here to take into account these errors is based on a correction factor $\overline{C}$ calculated from the average value of E_r obtained by averaging all data at a given F_i. A detailed discussion and justification of this approach can be found in [14].

$$\overline{C} = \frac{E_r^{reference}}{\overline{E}_r^{measured}} = \frac{\sqrt{A_{real\ contact}}}{\sqrt{A_c}} \tag{5}$$

The correction factor $\overline{C}$ is then applied to the average hardness $\overline{H}$ to get a corrected hardness value as:

$$H^{corr} = \frac{F}{A_{real\ contact}} = \overline{H}\,\overline{C}^2 \tag{6}$$

In the following, only corrected hardness values are presented. Note that the correction factor we used is around 0.8 to 0.9.

4. Results and discussion

The effect of the proton irradiations on the load-penetration depth curves is shown in Fig. 5. A consistent increase of the load with irradiation dose at a given penetration is observed.

The corrected hardness data H^{corr}, according to Eq. (6) are shown in Fig. 6 where the data are plotted against the average force for the unirradiated and the two irradiation conditions. The lines were calculated from Eq. (9) and Eq.(10) with P_y = 0.165 GPa (see below). H^{corr} represents the mean indentation pressure and, to keep the self-consistency with the equations of the modified-slip distance theory presented in section 2, H^{corr} is reported as P_m in this section. As expected, a decrease of the hardness is observed with the force up about 40 mN, beyond which the hardness data seems to become practically constant, in particular for the two irradiated conditions. This observation clearly reflects the fact that the relative contribution of the term k_1/a becomes very small with respect to the other terms at large penetration depth (see

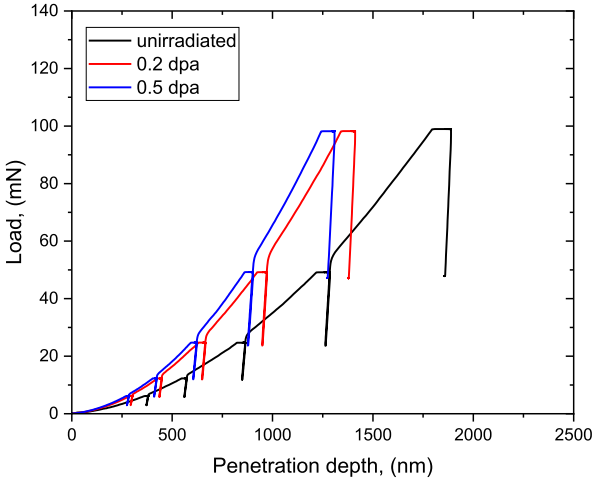

Fig. 5. Typical indentation loading curves before and after irradiation.

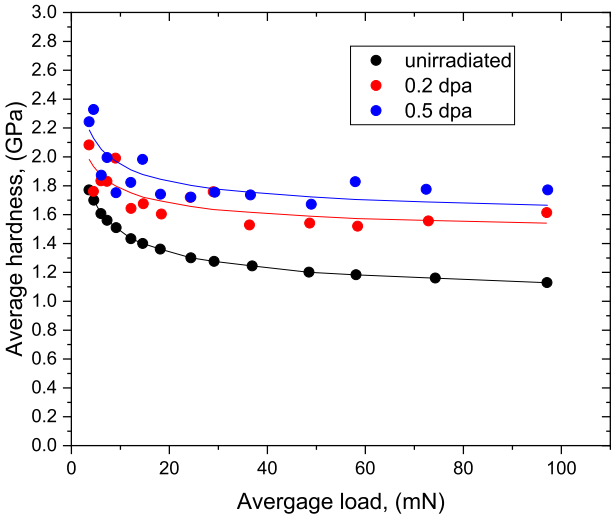

Fig. 6. Average hardness versus average load for the unirradiated and irradiated Fe9Cr.

Eq. (2)). A similar trend was already found by Hou et al. for a nanostructured metallic glasses [12]. However, the P_m data remain consistent with the fitted lines, and it is not obvious to confirm that P_m has really reached a constant value above 40 mN. Indeed, it is difficult to precisely define the load at which P_m would be considered constant, should it become because it would reach it asymptotically. Furthermore, the apparent constant value might be the consequence of the data averaging applied to correct the data. When looking at individual data set obtained on a single specimen loaded in PMC, a small but clear continuous decrease of the hardness is systematically observed for the three conditions. This is illustrated in Fig. 7 where uncorrected data for each condition are shown. Note also that the other PMC tests performed with a maximum force of 60 and 75 mN also show a decrease of hardness up to maximum force. So, the plateau in hardness is quite plausible to be reached for load somewhat higher than 100 mN.

For the analysis of the data in the frame of the modified slip-distance theory, three characteristic lengths were considered in Eq. (2) for the unirradiated and four irradiated material: i) the plastic zone size represented by the indentation contact radius a, ii) the grain size d, iii) the mean forest dislocation distance characterized by $1/\sqrt{\rho_s}$, and, iv) for the irradiated material, the mean distance between the irradiated defect (assumed to be spherical) with the volume density N and diameter δ. For convenience, Eq. (2) is rearranged as:

$$(P_m - P_y)^2 = \frac{k_1}{a} + \frac{k_2}{d} + k_3\sqrt{\rho_s^{unirr}} \qquad for\ unirradiated \tag{7}$$

$$(P_m - P_y)^2 = \frac{k_1}{a} + \frac{k_2}{d} + k_3\sqrt{\rho_s^{irr}} + k_4\sqrt{N\delta} \qquad for\ irradiated \tag{8}$$

As mentioned above, P_y is the stress to move dislocation in a defect-free crystal and represents the Peierls friction that we have to estimate. The tensile test data reported by Mueller on this Fe9Cr model alloy indicates a yield stress σ_y of 100 MPa [18]. This value is obviously greater than the yield stress of single crystal and is regarded as the upper limit. In order to examine the sensitivity of the different terms in Eq. (7) and (8), lower yield stresses (55 and 10 MPa) were also used in the analysis. P_y was obtained using Tabor's relationship that yield $P_y \approx 3\sigma_y$ [15]. In other words, P_y of 0.3 GPa, 0.165 GPa and 0.03 GPa were used to investigate the effect of P_y on the other parameters.

Since all the indentations were performed in the middle of a large grain, one can reasonably consider that single crystals were indented. Thus, $d = \infty$ and there is no contribution of the second term to consider in Eq. (7) and (8), which simplify to:

$$(P_m - P_y)^2 = \frac{k_1}{a} + k_3\sqrt{\rho_s^{unirr}} \qquad for\ unirradiated \tag{9}$$

$$(P_m - P_y)^2 = \frac{k_1}{a} + k_3\sqrt{\rho_s^{irr}} + k_4\sqrt{N\delta} \qquad for\ irradiated \tag{10}$$

Consequently, the discussion below is restricted to the values of k_1, $k_3\sqrt{\rho_{ss}}$, and $k_4\sqrt{N\delta}$. P_m and a being the experimental data, a plot of $(P_m\text{-}P_y)^2$ against a should be linear with a slope equal to k_1 with an intercept of $k_3\sqrt{\rho_s^{unirr}}$ for the unirradiated condition and with an intercept of $k_3\sqrt{\rho_s^{irr}} + k_4\sqrt{N\delta}$ for the irradiated conditions. The plots for the three material conditions are shown in Fig. 8, drawn with $P_m = 0.165$ GPa. At first glance, one observes that the slope of the three lines (k_1) is quite similar.

The precise values of the k_1 coefficients are reported in Table 1. Again, k_1 value accounts only for the contact radius effect and is reasonably constant for the three datasets. In addition, k_1 is not very sensitive to the choice of P_m.

For the unirradiated material, $k_3\sqrt{\rho_s^{unirr}}$ can be unambiguously determined as the intercept on the y-axis of the fit in Fig. 8, and it was found equal to 0.6102 GPa^2. $k_3\sqrt{\rho_s^{unirr}}$ represents the contribution of the dislocation density to the reduction of the mean free path of the mobile dislocations with respect to a defect-free crystal. For the irradiated

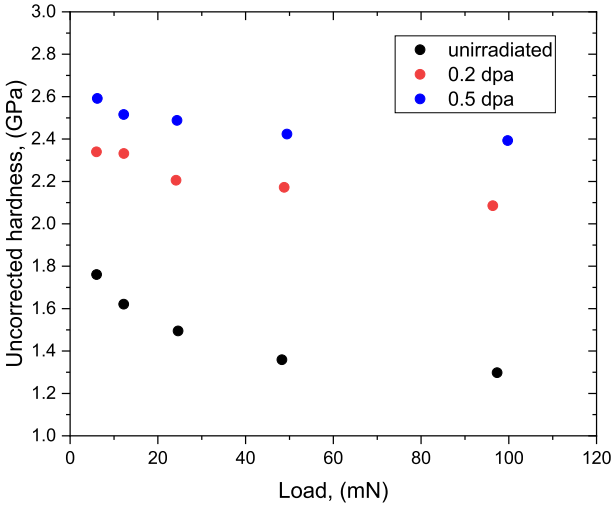

Fig. 7. Uncorrected hardness versus load for the unirradiated and irradiated Fe9Cr obtained in PMC.

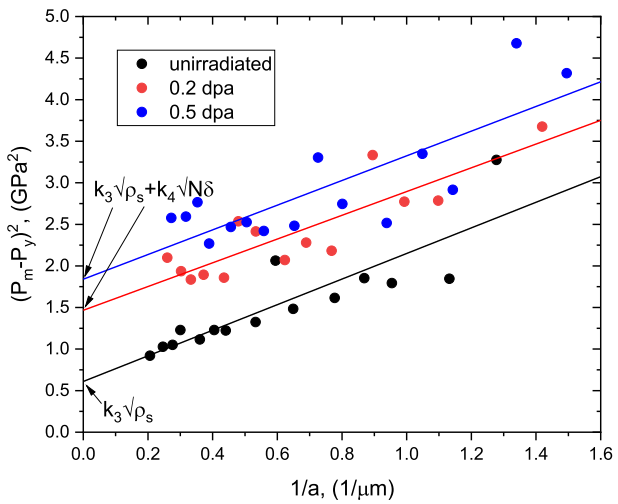

Fig. 8. Fit to the data using $P_m = 165$ MPa.

Table 1
K_1 values for different P_y values for the unirradiated and irradiated materials.

Specimen	k_1 for P_y = 300 MPa $[k_1]$ = GPa^{2}µm	k_1 for P_y = 165 MPa $[k_2]$ = GPa^{2}µm	k_1 for P_y = 30 MPa $[k_3]$ = GPa^{2}µm
unirradiated	1.3823	1.5395	1.6968
irr − 0.2 dpa	1.309	1.4282	1.5475
irr − 0.5 dpa	1.3745	1.4842	1.5939
average k_1	1.355 ± 0.033	1.484 ± 0.045	1.613 ± 0.062

material, the intercept on the y-axis is the sum of the two terms $k_3\sqrt{\rho_s^{irr}}$ + $k_4\sqrt{N\delta}$. With the information available from the tests, the relative contributions of the last two terms is not straightforward. Indeed, the immobilization processes of the mobile dislocations are linked to the presence of irradiation defects, which obviously affect their mobility. Thus, the value of dislocation density ρ_s generally depends on all the other individual length scales that mediate the dislocation slip distance, in our case it also depends on the mean distance between the irradiation defect given by $1/\sqrt{N\delta}$. Furthermore, without knowing the specific values of k_3 and k_4 the relative contribution of the two terms $k_3\sqrt{\rho_s}$ and $k_4\sqrt{N\delta}$ cannot be determined from the sole information obtained from the indentations. N, δ and ρ_s can be obtained experimentally but only sophisticated TEM observations and analysis based on dislocation visibility criteria allows to get a reasonable estimate of these quantities [16]. It remains that the difference for large penetration depth, for which k_1/a is zero, the increase of P_m is given by:

$$\Delta P_m = P_m^{irr} - P_m^{unirr} = \sqrt{\left(k_3\sqrt{\rho_s^{irr}} + k_4\sqrt{N\delta}\right)} - \sqrt{k_3\sqrt{\rho_s^{unirr}}} \quad (11)$$

which fully characterizes the irradiation hardening at infinitely large indent. ΔP_m can be used with Tabor's equation to determine the increase of the yield stress ($\Delta\sigma_y = \Delta P_m/3$) for a given irradiation conditions. Using Eq (11) and the intercept for the 0.2 dpa and 0.5 dpa lines (=1.4663 and 1.8401 GPa^2 respectively) and that for the unirradiated (=0.6102 GPa^2) yields the following irradiation hardenings: $\Delta\sigma_y \approx 143$ MPa after 0.2 dpa irradiation and $\Delta\sigma_y \approx 191$ MPa after 0.2 dpa irradiation. These two estimates of the hardening at the irradiation temperature used (<150 °C) are in good agreement with the trend report by Yamamoto et al. on a wide range of data obtained on 8-9Cr ferritic steel [17].

5. Summary and conclusions

Measurements of the indentation size effects were carried out on a Fe9Cr model alloy having an equiaxed microstructure with a relatively large grain size (≈ 80 µm) with respect to the indentation size. The indentation data were obtained on unirradiated specimens as well as on proton-irradiated specimens at two different doses, namely 0.2 and 0.5 dpa, at low irradiation temperature (<150 °C). The usual decrease of the measured hardness with the penetration depth was observed. It was analyzed in the frame of the modified slip theory, which is based on the combination of the different length scales, namely the indent size and the mean distance between different microstructural features, which control the dislocation mean free path and the stress required to plastically deform the material. With a characteristic mean free path, represented by the inverse of the reciprocal sum of all the specific characteristic lengths, it was possible to describe properly the decrease of the hardness with the applied load or penetration depth. From the extrapolation to infinitely large indent size, the irradiation hardening was estimated and found in good agreement with the general trend determined on a large database of 8-9Cr ferritic steels.

Declaration of competing interest

The authors declare the following financial interests/personal relationships which may be considered as potential competing interests: [Spatig reports financial support was provided by Swiss National Science Foundation. If there are other authors, they declare that they have no known competing financial interests or personal relationships that could have appeared to influence the work reported in this paper.].

Data availability

Data will be made available on request.

Acknowledgments

The financial support of the Swiss National Science Foundation (Grant 463 No. 200021_184695) is gratefully acknowledged.

References

[1] C. Cabet, F. Dalle, E. Gaganidze, J. Henry, H. Tanigawa, Ferritic-martensitic steels for fission and fusion applications, J. Nucl. Mater. 523 (2019) 510–537, https://doi.org/10.1016/j.jnucmat.2019.05.058.
[2] P. Spätig, J.-C. Chen, G.R. Odette, Chapter 11 - Ferritic and Tempered Martensitic Steels, in: G.R. Odette, S.J. Zinkle (Eds.), Structural Alloys for Nuclear Energy Applications, Elsevier, Boston, 2019, pp. 485–527, https://doi.org/10.1016/B978-0-12-397046-6.00011-3.
[3] X. Xiao, D. Terentyev, L. Yu, Model for the spherical indentation stress-strain relationships of ion-irradiated materials, J. Mech. Phys. Solids 132 (2019) 103694, https://doi.org/10.1016/j.jmps.2019.103694.
[4] M. Clozel, L. Kurpaska, I. Jóźwik, J. Jagielski, M. Turek, R. Diduszko, E. Wyszkowska, Nanomechanical properties of low-energy Fe-ion implanted Eurofer97 and pure Fe, Surf. Coat. Technol. 393 (2020) 125833, https://doi.org/10.1016/j.surfcoat.2020.125833.
[5] Y. Yang, D. Frazer, M. Balooch, P. Hosemann, Irradiation damage investigation of helium implanted polycrystalline copper, J. Nucl. Mater. 512 (2018) 137–143, https://doi.org/10.1016/j.jnucmat.2018.09.022.
[6] D.W. Nix, H. Gao, Indentation size effects in crystalline materials: a law for strain gradient plasticity, J. Phys. of Solids 46 (3) (1998) 411–425, https://doi.org/10.1016/S0022-5096(97)00086-0.
[7] G.I. Taylor, The mechanism of plastic deformation of crystals. Part I., Proc. R. Soc. Math. Phys. Eng, Sci. 145 (1934), 362-397, Doi: 10.1098/rspa.1934.0106.
[8] Y. Huang, F. Zhang, K.C. Hwang, W.D. Nix, G.M. Pharr, F. g., A model of size effects in nano-indentation, J. Mech. Phys. Solids 54 (2006), 1668–1686, Doi: 10.1016/j.jmps.2006.02.002.
[9] E. Demir, D. Raabe, N. Zaafarani, S. Zaefferer, Investigation of the indentation size effect through the measurement of the geometrically necessary dislocations beneath small indents of different depths using EBSD tomography, Acta Mater. 57 (2) (2009) 559–569, https://doi.org/10.1016/j.actamat.2008.09.039.
[10] D.J. Dunstan, B. Ehrler, R. Bossis, S. Joly, K.M.Y. P'ng, A.J. Bushby, Elastic Limit and Strain Hardening of Thin Wires in Torsion, Phys. Rev. Lett. 103(15) (2009), 155501, Doi: 10.1103/PhysRevLett.103.155501.
[11] X. Hou, N.M. Jennett, Application of a modified slip-distance theory to the indentation of single-crystal and polycrystalline copper to model the interactions between indentation size and structure size effects, Acta Mater. 60 (10) (2012) 4128–4135, https://doi.org/10.1016/j.actamat.2012.03.054.
[12] X. Hou, N.M. Jennett, M. Parlinska-Wojtan, Exploiting interactions between structure size and indentation size effects to determine the characteristic dimension of nano-structured materials by indentation, J. Phys. D Appl. Phys. 46 (26) (2013) 265301, https://doi.org/10.1088/0022-3727/46/26/265301.
[13] W.C. Oliver, G.M. Pharr, Measurement of hardness and elastic modulus by instrumented indentation: Advances in understanding and refinements to methodology, J. Mater. Res. 19 (1) (2004) 3–20, https://doi.org/10.1557/jmr.2004.19.1.3.
[14] A. Ruiz-Moreno, P. Hähner, L. Kurpaska, J. Jagielski, P. Spätig, M. Trebala, S.-P. Hannula, S. Merino, G. de Diego, H. Namburi, O. Libera, D. Terentyev, T. Khvan, C. Heintze, N. Jennett, Round Robin into Best Practices for the Determination of Indentation Size Effects, Nanomaterials 10 (1) (2020) 130, https://doi.org/10.3390/nano10010130.
[15] D. Tabor, The Hardness of Metals, Clarendon Press, Oxford, 1951.
[16] A. Prokhodtseva, B. Décamps, A. Ramar, R. Schäublin, Impact of He and Cr on defect accumulation in ion-irradiated ultrahigh-purity Fe(Cr) alloys, Acta Mater. 61 (18) (2013) 6958–6971, https://doi.org/10.1016/j.actamat.2013.08.007.
[17] T. Yamamoto, G.R. Odette, H. Kishimoto, J.-W. Rensman, P. Miao, On the effects of irradiation and helium on the yield stress changes and hardening and non-hardening embrittlement of ~8Cr tempered martensitic steels: Compilation and analysis of existing data, J. Nucl. Mater. 356 (1) (2006) 27–49, https://doi.org/10.1016/j.jnucmat.2006.05.041.
[18] P. Mueller, PhD Thesis, Nr. 4518, EPFL, Ecole Polytechnique Fédérale de Lausanne, (2009).